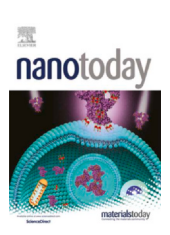
\$ \$ \$ ELSEVIER

Contents lists available at ScienceDirect

Nano Today

journal homepage: www.elsevier.com/locate/nanotoday



On-demand synthesis of antiseptics at the site of infection for treatment of otitis media



Jiayan Lang ^{a,1}, Xiaojing Ma ^{a,1}, Sophie S. Liu ^{a,b}, Danielle L. Streever ^b, Max D. Serota ^a, Trevor Franklin ^a, Ellis R. Loew ^c, Rong Yang ^{a,*}

- ^a Robert F. Smith School of Chemical & Biomolecular Engineering, Cornell University, Ithaca, NY 14853, USA
- ^b Meinig School of Biomedical Engineering, Cornell University, Ithaca, NY 14853, USA
- ^c College of Veterinary Medicine, Cornell University, Ithaca, NY 14853, USA

ARTICLE INFO

Article history: Received 20 March 2022 Received in revised form 14 September 2022 Accepted 30 October 2022 Available online xxxx

Keywords:
On-demand synthesis
Antiseptics
Vanadium pentoxide nanowire
Haloperoxidase-like activity
Otitis media

ABSTRACT

Otitis media (OM) is the main reason for pediatric antibiotic prescriptions. The current treatment mandates a rigorous regimen of multidose antibiotics over 5–10 days. The systemic antibiotic exposure and often prematurely terminated treatment due to the challenge of drug administration to young patients are believed to breed antibiotic resistance. To address these challenges, we designed a local treatment that converted a metabolic product (H_2O_2) of an OM pathogen (Streptococcus pneumoniae) into a potent antiseptic (HOBr), a reaction catalyzed by locally administered vanadium pentoxide nanowires. The therapeutic, HOBr, was only synthesized in the presence of the pathogen, enabling on-demand generation of therapeutics for OM treatment. Hypohalous acids are broad-spectrum and have a long history in general disinfection applications without breeding substantial drug resistance. A single dose of the nanowire formulation eradicated OM in a standard chinchilla model in 7 days with no observable tissue toxicity or negative impact on hearing sensitivity.

© 2022 Elsevier Ltd. All rights reserved.

Introduction

Every year, 12 million to 16 million physician visits in the United States (U.S.) are attributed to otitis media (OM), the most common specifically treated childhood disease [1]. Over 95 % of children in the U.S. have at least 1 episode of acute OM, with one third of them experiencing 6 or more episodes by age 7 [2]. Streptococcus pneumoniae (S. pneumoniae) and nontypeable Haemophilus influenzae (NTHi) are two of the most common OM pathogens worldwide, which are responsible for ~35 % and ~23 % of all OM cases respectively [3]. Other pathogens include Moraxella catarrhalis (accounting for ~14 % of OM cases) and ones that are rare in OM such as

Abbreviation: OM, Otitis Media; NTHi, Nontypeable Haemophilus influenzae; MIC, minimum inhibitory concentration; NWs, nanowires; ABR, auditory brainstem response; ROS, reactive oxygen species; TOF, turnover frequency; $K_{\rm m}$, Michaelis-Menten constant, $V_{\rm max}$: maximum reaction rate; MEF, middle ear fluid; TM, tympanic membrane; CPE, chemical permeation enhancer; BHI, brain heart infusion; hFBs, Human primary dermal fibroblasts; FBM, Fibroblast Basal Medium; HBSS, Hanks' balanced salt solution

pseudomonas aeruginosa (PAO1), alpha-hemolytic Streptococcus, group A Streptococcus (GAS), and Staphylococcus aureus (S. aureus) each of which accounts for $\sim 1-3\%$ of all OM cases [3]. Unfortunately, current therapy for acute OM requires adherence to a rigorous outpatient regimen of multiple doses of antibiotics per day over 5–10 days, the adherence to which in young children remains challenging partially due to the severe side effects observed in over 50 % of U.S. children [4]. As a result, treatments are often terminated once symptoms are resolved while pathogens may still be present, leading to recurrent OM and rapid development of antimicrobial resistance [5,6]. For example, in *S. pneumoniae*, one of the major OM pathogens causing approximately 300 million OM cases annually worldwide (corresponding to 30-50 % of all OM cases) [7], reduced susceptibility or resistance to ß-lactam and macrolide antibiotics has become prevalent among the clinical isolates [8-10]. The minimum inhibitory concentration (MIC) of S. pneumoniae is among the highest in OM pathogens. The MIC of ciprofloxacin against certain strains of *S. pneumoniae* is as high as $0.5-4 \mu g/mL$, over 50 times that of NTHi (another common OM pathogen with MIC of less than 0.01 ug/mL for ciprofloxacin) [9.11]. Furthermore, 30 % of severe S. pneumoniae infections are untreatable by one or more antibiotics because of the rapid development of drug resistance [12], which is

Corresponding author.

E-mail address: ryang@cornell.edu (R. Yang).

¹ These authors contributed equally to this work.

further exacerbated by the prevalence of OM. Responsible for 21 % of all antibiotic prescriptions written to U.S. children [13], acute OM is believed to contribute substantially to the ongoing increase in antimicrobial resistance identified among nasopharynx pathogens in the general public [14].

In contrast to the rapid development of resistance to antibiotics, hypohalous acids are used extensively in healthcare and water disinfection since 1854 and without substantial resistance documented to date [15]. They have demonstrated broad-spectrum antimicrobial effects against viruses, bacteria, and fungi [16]. Tolerance of OM pathogens towards hypobromous acid (HOBr) has not been reported to our best knowledge. Although hypohalous acids have negligible tissue toxicity at effective concentrations (10-100 µg/mL) [15], a fundamental challenge for their application as a therapeutic is the short half-life in vivo [16], which prevents the sustained antimicrobial effects required to treat conditions like OM. In this report, we address this challenge by generating hypohalous acids in situ using a catalytic nanozyme based on vanadium pentoxide nanowires (V₂O₅ NWs). The V₂O₅ NWs not only mimic the reactivities of vanadium haloperoxidases (V-HPOs) enzymes isolated from the marine algae Macrocystis pyrifera [17], which has been discovered to have sustained antimicrobial activities. Furthermore, the cylindrical shape of the V₂O₅ NWs is highly desirable for achieving long retention time in the auditory bullae as such non-isotropic shape is known to increase the radius of gyration and thus decrease diffusivity in body fluids [17] (like middle ear fluid).

To treat infections caused by the OM pathogen, S. pneumoniae, we synthesized V₂O₅ NWs that convert a known metabolic product of S. pneumoniae, hydrogen peroxide (H2O2), to hypohalous acid continuously and catalytically (i.e., without consumption of V_2O_5 NWs). While the basal level of H_2O_2 in human plasma is close to zero [18], S. pneumoniae produces up to 1 mM H₂O₂ per hour during log-phase growth due to its pyruvate oxidase activity [19], sufficiently fueling the production of hypohalous acid by V₂O₅ NWs. In addition, the inflammation caused by S. pneumoniae-induced OM could further promote that catalytic generation of antimicrobials by (i) generating the middle ear fluid, which in turn provides a liquid environment to enable the catalytic activity of V₂O₅ NWs; and (ii) supplies additional H₂O₂ generation sources like phagocytic cells [20,21] which could generate nanomolar-levels of H₂O₂ [22]. As a result, the synthesis of hypohalous acid only occurs in the presence of S. pneumoniae, and stops upon cure of OM, thus ensuring the on-demand treatment of infections caused by S. pneumoniae while minimizing the tissue exposure to hypohalous acid and associated side effects [23]. That continuous generation of hypohalous acid in response to an active episode of OM potentially enables a single application of the V₂O₅ NWs formulation to cure recurrent infections.

Here, we demonstrate the successful treatment of *S. pneumoniae* OM in an established chinchilla animal model [24], using a singledose formulation containing the V₂O₅ NWs. The formulation eradicated acute OM in chinchillas within 7 days and demonstrated excellent biocompatibility in the ear. Detailed studies on the catalytic reaction kinetics confirmed that the V₂O₅ NWs enabled the oxidation of bromide (Br⁻) into HOBr leveraging the H₂O₂ produced by S. pneumoniae, the catalytic activity of which was captured by the Michaelis-Menten model. The in vitro antibacterial efficacy of the V₂O₅ NWs was assessed using a clinical isolate of S. pneumoniae, which demonstrated complete eradication of the bacteria in culture media in the presence of 1 mM Br⁻. Building upon these promising in vitro results, we proceeded to testing the nanozyme's efficacy where chinchillas were infected with the S. pneumoniae and treated via a single intrabulla injection of a formulation containing 0.08 mg/mL V₂O₅ NWs and 1 mM Br⁻. The number of colony-forming units (CFU) in the middle ear of the infected animals was reduced by more than 10,000 times, 7 days after the injection. Due to the primitive immune system of chinchillas, a 3-log reduction in the middle ear CFU

count is commonly considered to translate to complete cure in human children [25,26], which was far exceeded by the reported nanozyme formulation here. Furthermore, excellent biocompatibility of the nanozyme formulation was demonstrated via auditory brainstem response (ABR) testing, the results of which were identical in animals treated by the formulation and healthy, untreated animals. Auditory bullae harvested from treated animals also appeared histologically similar to untreated ones, further corroborating the biocompatibility of the treatment. The biocompatibility was likely a result of the on-demand generation of antiseptics, which was active only in the presence of *S. pneumoniae*, thus preventing potentially toxic overexposure to HOBr.

This design enabled on-demand synthesis of therapeutics at the site of infection, which represents a new paradigm in infectious disease treatment. The broad-spectrum antimicrobial effects of hypohalous acids against viruses (e.g., anti-HIV), bacteria, and fungi [16], their record of low probability of developing drug resistance, and the emerging health benefits (e.g., cytoprotective and anti-inflammatory effects [27]) point to the broad deployment of this strategy in the treatment of infections involving reactive oxygen species (ROS)-generating pathogens. It has the potential to curb the development of antimicrobial resistance, one of the greatest global public health concerns, and mitigate the 35,000 deaths, 2.8 millions hospitalizations, and \$20-billion of additional medical expenditures associated with antibiotic resistant infections [28,29].

Results

Single-crystalline V₂O₅ NWs were synthesized

 V_2O_5 NWs were synthesized using a hydrothermal approach based on previous reports [30,31]. The as-synthesized V_2O_5 NWs were characterized for detailed information on the particle geometry, crystallography, elemental composition, and bonding environments as described below.

Transmission electron microscopy (TEM) illustrated the elongated geometry of the V₂O₅ NWs, with an average length of 404.7 ± 166.6 nm and an average width of 35.6 ± 10.4 nm (Fig. 1A and Supplementary Fig. S1). These dimensions were consistent with previous reports that employed the hydrothermal synthesis approach [30]. High-resolution transmission electron microscopy (HRTEM) imaging demonstrated the typical orthorhombic lattice structure of V_2O_5 NWs with a distance of ~ 0.270 nm between the nearest neighboring plane (Fig. 1B), which is considered to enable the HPO-like activities of V₂O₅ NWs. This lattice parameter was consistent with the reported distance between the (040) planes of an orthorhombic lattice in V₂O₅, thus confirming that the nanowire grew along the [010] direction as described previously [32]. The [010] lattice plane of V₂O₅ NWs is important because it displays a vanadium coordination geometry similar to that of the active site of V-HPO (identified in Macrocystis pyrifera) [27]. The fast Fourier transform (FFT) of HRTEM (Fig. 1C) (taken from an individual nanowire) and X-ray diffraction (XRD) patterns (Supplementary Fig. S2) revealed the single-crystalline nature of the V_2O_5 NWs.

Scanning transmission electron microscopy with energy dispersive X-ray spectroscopy (STEM-EDX) provided the elemental mapping that further demonstrated uniform distributions of V and O in the V_2O_5 NWs (Fig. 1D, F), with the O:V ratio of ~2.5, as calculated from the EDX spectrum (Supplementary Fig. S3). The atomic percentage of O and V collected from the EDX spectrum were ~68.08 % and ~27.73 %, respectively, consistent with the theoretical atomic ratio in V_2O_5 . That elemental composition was corroborated by a survey scan performed using X-ray photoelectron spectroscopy (XPS) (Fig. 1G). To confirm that the correct bonding environment was obtained for the V_2O_5 NWs, XPS high-resolution scans on V (2p) and O (1s) were performed with the peaks deconvoluted using

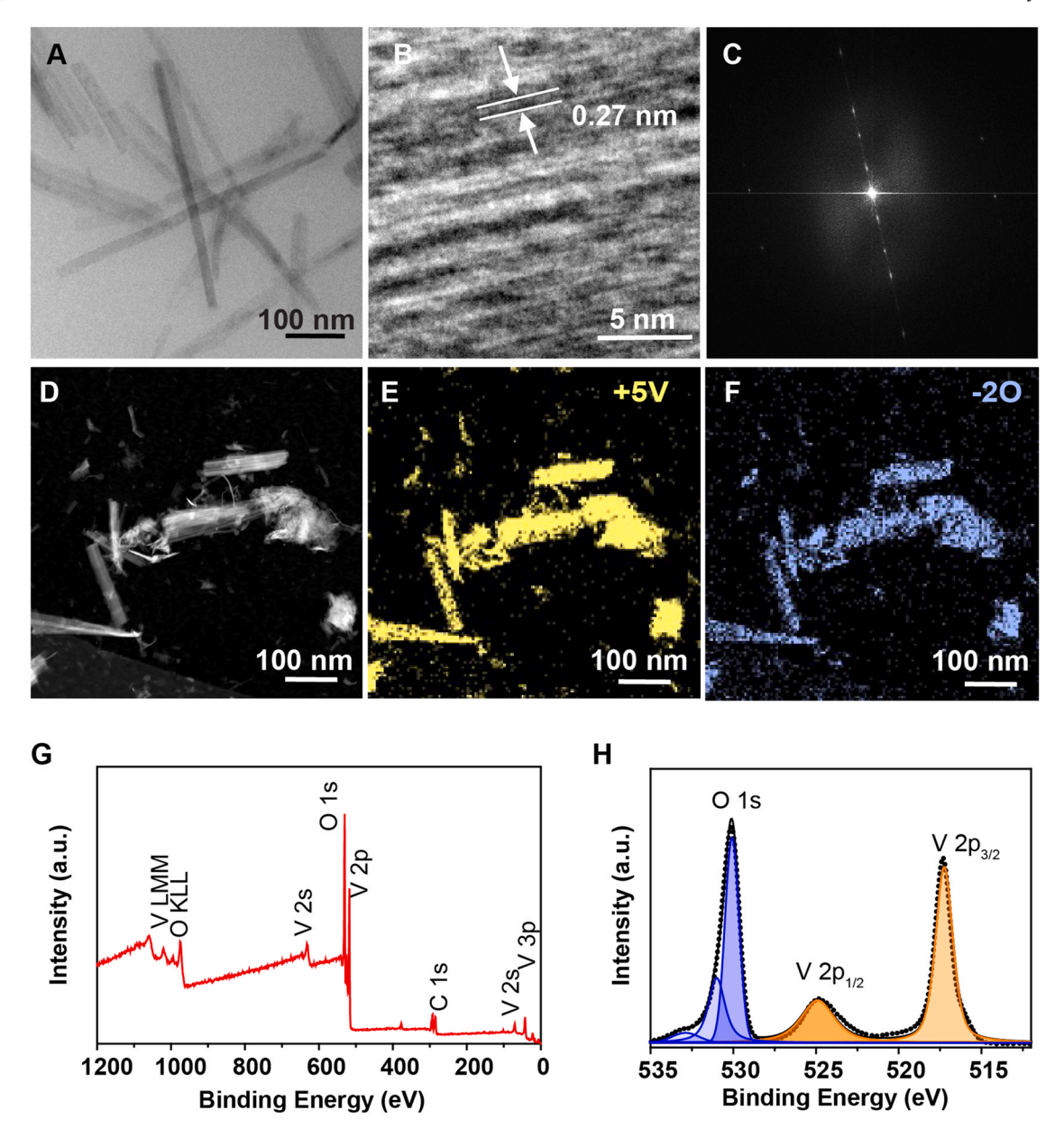


Fig. 1. Characterization of the V_2O_5 NWs. (A, B) TEM and HRTEM images of the V_2O_5 NWs. (C) FFT of the HRTEM image of a single V_2O_5 NW. (D-F) the STEM image (D) and the corresponding EDX elemental mapping of V (E) and O (F). (G) XPS survey scan of the V_2O_5 NWs. (H) High-resolution XPS spectra of the V_2O_5 NWs with deconvoluted core level spectra of O(1 s) (blue peaks) and V(2p) (orange peaks). The black solid line corresponds to the envelope/fitting curve, and the black dots represent the raw data.

Lorentzian–Gaussian functions. The peaks at 517.2 eV and 524.9 eV corresponded to the spin-orbit split of V 2p3/2 and V 2p1/2 (Fig. 1H, orange peaks), respectively, indicative of the valence state of V(V) [33,34]. The high-resolution XPS scan on O (1 s) (Fig. 1H, blue peaks), revealed that the dominating oxygen species was the lattice oxygen, captured at ~ 530.1 eV, constituting 62.7 % of the total oxygen. Other oxygen species mainly comprised (i) the -OH groups on the surface of the V₂O₅ NWs, with the binding energy of ~ 531 eV, constituting ~ 31.4 % of the total oxygen, and (ii) surface-adsorbed water (~ 6.0 % of the total oxygen), with the binding energy of ~ 532.8 eV [34]. These materials characterization results confirmed the geometry and chemical composition of the as-synthesized V₂O₅ NWs, proved their crystallinity, and quantified their lattice parameters, based on which the catalytic activities were characterized in detail as described below.

V₂O₅ NWs demonstrated catalytic activities comparable to the V-HPOs

The haloperoxidase-like catalytic activities of V₂O₅ NWs were quantified using a colorimetric assay, i.e., the phenol red (PR, phenolsulfonphthalein) bromination assay, which is commonly used to quantify the concentration of HOBr in an aqueous solution [35]. Generation of HOBr, via the haloperoxidase-like activities of V₂O₅ NWs, has been demonstrated to be the rate-limiting step in the colorimetric reaction cascade [36], which was confirmed by our observation that the bromination rate of PR was independent of the PR concentration (Supplementary Fig. S4). Using UV-vis spectrophotometer, the bromination of PR (using a 25 μ M aqueous solution of PR, with light absorbance at 430 nm) to bromophenol blue (Br₄PR, 3',3",5',5"-tetrabromophenolsulfonphthalein, with light absorbance at 590 nm) was observed in the presence of V₂O₅ NWs, Br⁻ and H₂O₂ (Fig. 2 A), whereas no bromination occurred in the absence of V_2O_5 NWs, or Br⁻ or H_2O_2 (Fig. 2B). The initial rate (v_0) of the bromination reaction, which was indicative of the rate of HOBr generation, was

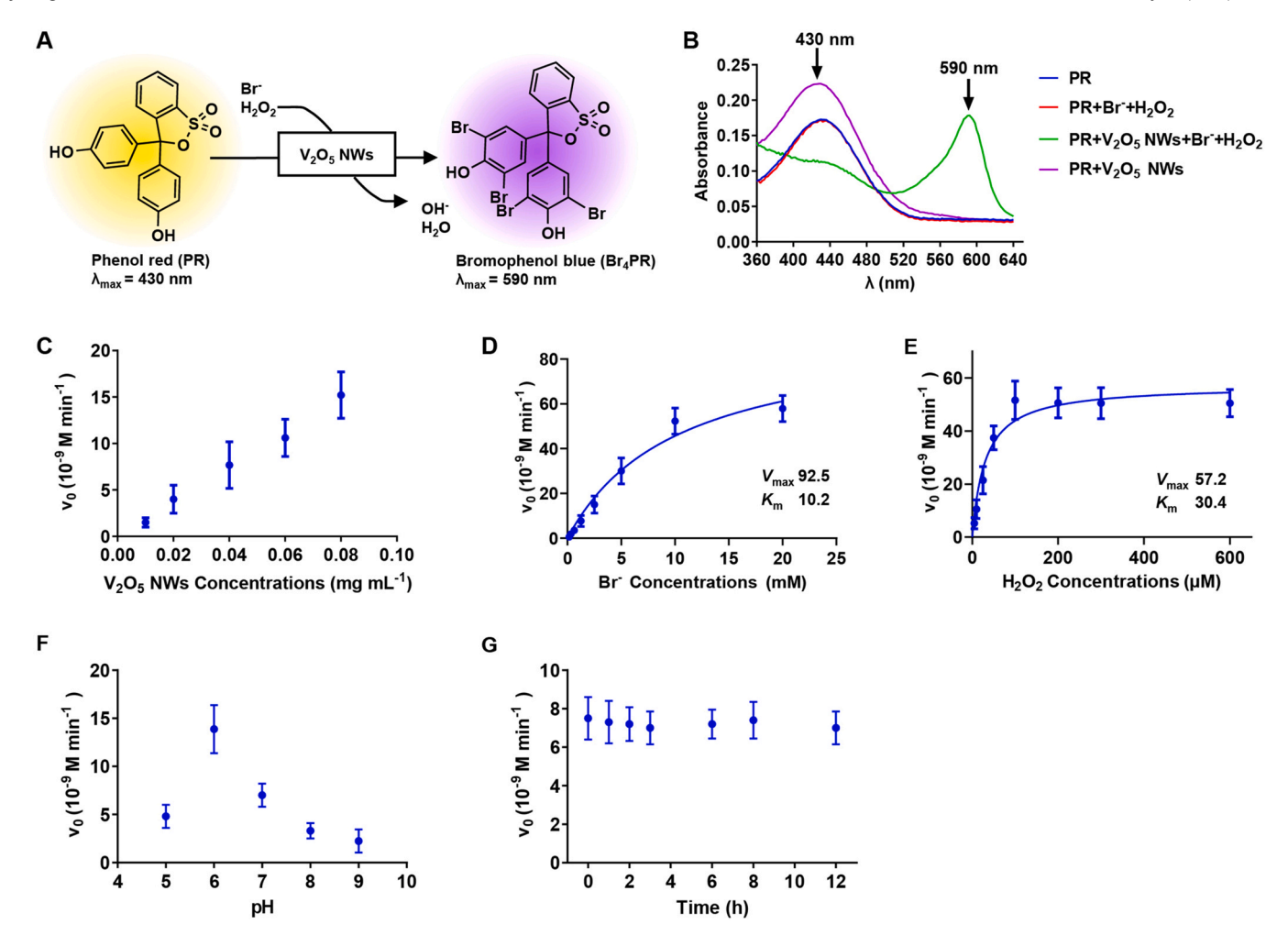


Fig. 2. Catalytic activities of the V_2O_5 NWs. (A) Scheme of the oxidative bromination reaction (converting PR to Br_4PR), used to quantify the reaction kinetics of HOBr generation. (B) UV–vis spectra demonstrating the bromination reaction only in the presence of V_2O_5 NWs, Br^- , and H_2O_2 . The reaction mixtures contained $25 \,\mu\text{M}$ PR, and/or $0.04 \,\text{mg/mL} \,V_2O_5$ NWs, and/or $1 \,\text{mM} \,Br^-$, and/or $100 \,\mu\text{M} \,H_2O_2$; the spectra were collected in triplicates after $12 \,\text{h}$ of reaction time. (C) Dependence of the initial rate of the bromination reaction on the concentration of V_2O_5 NWs, collected at the Br^- concentration of $10 \,\mu\text{M}$. (D) Dependence of the initial rate of the bromination reaction on the concentration of Br^- , collected at the V_2O_5 NWs concentration of $0.04 \,\text{mg/mL}$ and the Br^- concentration of $10 \,\mu\text{M}$. (E) Dependence of the initial rate of the bromination reaction on the concentration of V_2O_5 NWs concentration of V_2O_5 NWs was V_2O_5

quantified experimentally using the time-evolution of the absorbance of Br_4PR at 590 nm (A_{590}) (Eq. 1), based on the Lambert-Beer equation (Eq. 2).

$$v_0 = \frac{d[Br_4PR]}{dt} \tag{1}$$

$$[Br_4PR] = \frac{A590}{d \cdot \varepsilon_{BR_4PR}} \tag{2}$$

Theoretically, the initial rate (v_0) of this catalytic reaction follows the Michaelis-Menten equation (Eq. 3) [35].

$$v_0 = V_{max} \frac{[S]}{K_m + [S]} = k_{cat} [E]_0 \frac{[S]}{K_m + [S]}$$
(3)

where [S] is the concentration of the substrate (i.e., Br or H_2O_2) and [E] is the concentration of the nanozyme (V_2O_5 NWs). Indeed, the initial rate (v_0) demonstrated a linear dependence on the concentration of V_2O_5 NWs (Fig. 2 C), which is consistent with the predictions made in the Michaelis-Menten model with respect to the enzyme concentration (i.e., $v_0 = k_{\rm cat}[E]$, when [S] is kept constant; $k_{\rm cat}$, the turnover frequency (TOF), the number of reacted molecules to that of an active site). To measure the Michaelis-Menten constant

 $(K_{\rm m})$, which describes the binding affinity of a substrate (i.e., Br $^-$ or H $_2$ O $_2$) to the V $_2$ O $_5$ NWs and the maximum reaction rate $(V_{\rm max})$ for a certain V $_2$ O $_5$ NWs concentration, we individually varied the concentrations of the substrates, while keeping concentrations of V $_2$ O $_5$ NWs and PR constant at 0.04 mg/mL and 25 μ M, respectively. The values of $K_{\rm m}$ and $V_{\rm max}$ were obtained from the experimental data (Fig. 2D, E), using the Lineweaver-Burk linearization (Eq. 4):

$$\frac{1}{v_0} = \frac{K_m}{V_{max}} \cdot \frac{1}{[S]} + \frac{1}{V_{max}} \tag{4}$$

As such, the $K_{\rm m}$ values were determined to be 30.4 μ M for H₂O₂ and 10.2 mM for Br⁻, respectively, implying the concentration of H₂O₂ that was secreted by *S. pneumoniae* (up to 1 mM as reported [37] and based on our test) is enough to sustain the catalytic reaction. The $V_{\rm max}$ value was determined to be 57.2–92.5 × 10⁻⁹ M min⁻¹ for the V₂O₅ NWs at concentration of 0.04 mg/mL. The TOF (or $k_{\rm cat}$ reflecting the activity of a catalyst) was calculated to be 1.7 × 10⁻³ min⁻¹ for the as-synthesized V₂O₅ NWs (where $k_{\rm cat}$ was taken as the $V_{\rm max}$ for the molar concentration of the catalyst).

The aforementioned kinetic parameters were consistent with those reported in the literature for V_2O_5 NWs (e.g., K_m was reported to be 10 μ M for H_2O_2 by F. Natalio and W. Tremel [30]). They were

also consistent with the kinetic parameters reported for the biological enzyme, V-HPOs (e.g., vanadium chloroperoxidase found in Curvularia inaequalis was reported to have a $K_{\rm m}$ value of 3.1 mM for Br⁻ [38], and vanadium bromoperoxidase found in Ascophyllum nodosum was reported to have a $K_{\rm m}$ value of 18.1 mM for Br-). The readers are referred to Supplementary Table S1 for a detailed comparison with the literature values [39].

V₂O₅ NWs retained catalytic activity in the pH range relevant to OM treatment and over the course of at least 12 h. Based on past research that demonstrated V-HPOs enzymes to have greater catalytic activities in acidic environments [40], the effect of pH on the V₂O₅ NWs was examined by varying the pH of the solution in the range of 5-9 while measuring the catalytic activities as described above. This pH range was chosen to cover (i) the range of pH for the culture of S. pneumoniae, which varies between 6.5 and 8.3 depending on the culture time [41] and (ii) the range of pH of the middle ear fluid (MEF) during an episode of OM, which has been reported to range between 7.0 and 8.5 [42]. Using a solution containing $0.04 \text{ mg/mL V}_2\text{O}_5 \text{ NWs}$, 1 mM Br⁻, and $10 \,\mu\text{M}\,\text{H}_2\text{O}_2$, the pH under which the maximum catalytic activities were observed for the as-synthesized V_2O_5 NWs was measured to be ~6 (Fig. 2 F), with a v_0 value of $13.9 \pm 2.5 \times 10^{-9}$ M min⁻¹. At the pH of 7, approximately 50.5 ± 8.6 % of that maximum reactivity was retained, which further decreased to 23.9 \pm 5.7 % at the pH of 8.

The sustained catalytic behavior is required of V_2O_5 NWs to achieve complete eradication of OM. Therefore, we assessed performance of the V_2O_5 NWs over the course of 12 h, using a solution containing 1 mM Br⁻, 10 μ M H $_2O_2$, and 0.04 mg/mL V_2O_5 NWs. The V_2O_5 NWs demonstrated unchanged catalytic activities throughout the monitored 12-hour period (Fig. 2 G). These reaction kinetics studies demonstrated that the V_2O_5 NWs was able to retain catalytic activities over the pH range of 5–9, and over the course of 12 h. Based on these results, we anticipated the V_2O_5 NWs to demonstrate catalytic activities under the conditions relevant to the in vitro and in vivo assessments for antibacterial efficacy and biocompatibility as described below.

V₂O₅ NWs/Br- formulation eradicated S. pneumoniae in vitro

To assess the effectiveness of the V₂O₅ NWs to convert the bacteria-produced H₂O₂ to HOBr and thus eradicate the bacteria, we used a clinically isolated OM pathogen, S. pneumoniae, which excretes H₂O₂ as a metabolic product. The concentration of H₂O₂ generated by S. pneumoniae after overnight culture (12-16 h) was ~1 mM in the supernatant, assessed using a fluorometric method based on an H₂O₂ probe (10-acetyl-3,7-dihydroxyphenoxazine, ADHP). In contrast, H₂O₂ cannot be detected in the culture treated with the formulation (i.e., V2O5 NWs and Br-) because the nanomaterials interfered with the reading of the ADHP assay. In addition, the catalytic reactions consume H₂O₂ while eradicating S. pneumoniae, which serves as the main generator of H2O2, thus further diminishing H_2O_2 in the treated culture (as shown in Fig. 3). Building upon the H₂O₂-generating capability of S. pneumoniae, we demonstrated that its growth was inhibited entirely in the presence of 0.04 mg/mL V₂O₅ NWs and 1 mM Br⁻, without the need to introduce exogeneous H₂O₂ (Fig. 3 A). The antimicrobial efficacy remained unchanged upon addition of H2O2 to the final concentration of $20\,\mu\text{M}$, (i.e., treating the culture with a combination of $0.04\,\text{mg/mL}$ V_2O_5 NWs, 1 mM Br⁻, and 20 μ M H_2O_2). A suppression effect on the bacterial growth was also observed in the group containing 0.04 mg/ mL V₂O₅ NWs only, corresponding to a stationary-phase OD600 that is 25.8 % that of the non-treated culture after 15 h. For the group treated with 1 mM Br⁻ and 20 µM H₂O₂, the stationary-phase OD600 was also mildly reduced to 94.5 % that of the non-treated group after 15 h. We note that growth curves based on OD600 may not reflect bacterial survival with complete fidelity as dead cells and cell debris

could contribute to the OD600 readings via light scattering. Therefore, to confirm the viability of S. pneumoniae after the aforementioned treatments, an aliquot ($100 \,\mu L$) of the liquid culture (at the end of the 15-hour incubation), was plated onto blood agar to assess the CFU count (Fig. 3B). Although the high densities of bacteria prevented a qualitative assessment of the CFU count under several treatment conditions, a clear difference was observed between the groups treated with 0.04 mg/mL V₂O₅ NWs +1 mM Br⁻ or with $0.04 \text{ mg/mL V}_2\text{O}_5 \text{ NWs} + 1 \text{ mM Br}^- + 20 \,\mu\text{M} \,\text{H}_2\text{O}_2$, where no bacteria growth was observed, and those that were nontreated, or treated with 1 mM Br⁻ + 20 μ M H₂O₂, or with 0.04 mg/mL V₂O₅ NWs alone, where colonies were too dense to quantify. Next, the antimicrobial effect of another HPO-mimicking nanomaterial, cerium oxide nanorods (CeO_{2-x} NRs), was tested against S. pneumoniae as a comparison with the V₂O₅ NWs (Supplementary Fig. S5). Notably, the CeO_{2-x} NRs only partially inhibited the growth of S. pneumoniae at 0.08 mg/mL, the maximum concentration of either nanoparticle tested, and complete inhibition was not observed. This can be understood through the greater catalytic activities demonstrated by CeO_{2-x} NRs in acidic environments (than that in pH-neutral solution), as reported previously[30]. These results indicated that V₂O₅ NWs were optimal in this case and were effective at converting the H₂O₂ produced by S. pneumoniae, an OM pathogen that has been challenging to treat, into a potent antimicrobial, HOBr, which in turn eradicated the pathogen, in lieu of conventional antibiotics. Their catalytic activities compare favorably to those of another candidate in the class of catalytic transition metal oxides, i.e., CeO_{2-x} NRs.

V₂O₅ NWs/Br- formulation was biocompatible in the ear

The cytotoxicity of V_2O_5 NWs was assessed in two cell lines which are representative of the cell types present in the auditory system: human dermal fibroblasts (hFBs) and PC12 Adh (a pheochromocytoma cell line used for testing neurotoxicity). After 24 h of incubation with the various formulations (as detailed below), the live and dead cells were stained and counted by the LIVE/DEAD staining kit (Fig. 4, A, B). No discernable cytotoxicity was captured in either hFBs or PC12 cells for the formulation containing 0.01 mg/mL V_2O_5 NWs (with 1 mM Br and 20 μ M H_2O_2). Nevertheless, mild cytotoxicity was observed after increasing the concentration of V_2O_5 NWs to 0.04 mg/mL. The cell survival rate at 0.04 mg/mL V_2O_5 NWs groups was reduced to 78.4 \pm 7.0 % for hFBs and 56.1 \pm 6.7 % for PC12.

The in vivo biocompatibility of the V₂O₅ NWs formulation was examined through two approaches: the ABRs test and tissue histological analyses, both performed on chinchillas. Chinchillas have been used as the benchmark animal model in OM research because their hearing range largely overlaps with that of humans [43] and the pathogenicity of OM in chinchillas largely resembles that in human children [44]. The chinchillas have large, accessible tympanic bulla with the total volume between 1.52 and 2.09 mL [45]. Considering the concentration of V₂O₅ NWs that we demonstrated to be antimicrobial (i.e., > 0.01 mg/mL) and the concentration that showed no observable cytotoxicity (i.e., $< 0.04 \, mg/mL$), we chose a formulation that contains 0.08 mg/mL V₂O₅ NWs for in vivo experiments. That would lead to a V_2O_5 NWs concentration of ~ 0.013 mg/mL in the auditory bullae of infected animals (upon intrabulla administration of a formulation volume of $200\,\mu L)$ due to dilution by MEF (assuming a MEF volume of $\sim 1 \text{ mL}[44,45]$). We predict that V_2O_5 NWs concentration in bullae to effectively eradicate in vivo bacterial growth, while maintaining optimum biocompatibility. Although a higher V₂O₅ NWs concentration (e.g., 0.16 mg/mL) would likely lead to greater antimicrobial effect (because v_0 increases linearly with the V₂O₅ NWs concentration as shown in Fig. 2C), it would also entail greater cytotoxicity based on Fig. 4 A&B.

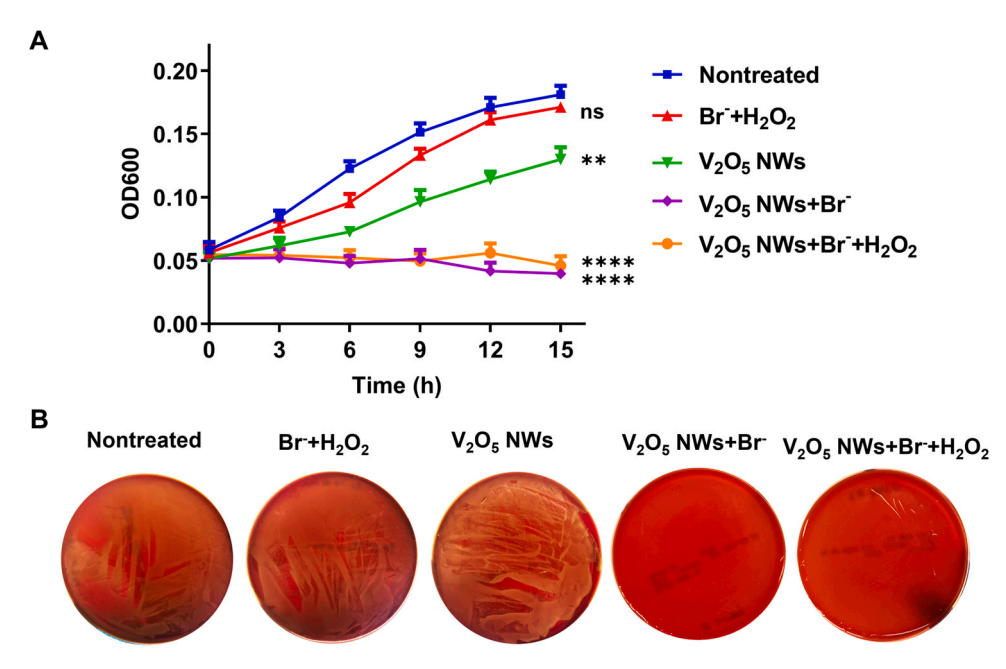


Fig. 3. Antibacterial effect of the V_2O_5 NWs. (A) Bacterial growth curves of *S. pneumoniae*. The OD600 was monitored for 15 h, where the initial concentration of V_2O_5 NWs was 0.04 mg/mL, of Br⁻ was 1 mM, and of H_2O_2 was 20 μ M. Data are mean \pm SD. (n = 4). ns, not statistically significant, ** p < 0.01, *** ** p < 0.001; all comparisons were made with respect to the "Nontreated" group. (B) Images of the blood agar plates obtained by plating the *S. pneumoniae* cultures at the end of the incubation shown in (A).

The value of ABR threshold reflects the hearing sensitivity, which is an important criterion for the assessment of ototoxicity [46]. To assess the effect of the V_2O_5 NWs treatment on hearing sensitivity, $200\,\mu\text{L}$ of the formulation containing $0.08\,\text{mg/mL}\,V_2O_5$ and $1\,\text{mM}\,\text{Br}^-$ was administered through the dorsal side of the auditory bullae of a healthy chinchilla, and the ABR threshold was measured before the injection, and $20\,\text{mins}$, $1\,\text{day}$, $3\,\text{days}$ and $6\,\text{days}$ post-injection. The ABR threshold measured prior to the injection of V_2O_5 NWs for each animal was used as a baseline for the normalization of subsequent measurements.

After an initial minor increase of the click ABR threshold by $1.2 \pm 1.5 \, dB$ at 20 min after the treatment, hearing sensitivity of the treated chinchillas remained unchanged over the course of the 6-day treatment at values comparable to those of healthy and untreated animals (Fig. 4C). Furthermore, wave II of the measured ABR response, the wave with the most obvious amplitude (among waves I, II, III, and IV) was examined to assess effect of the formulation on synchronous neural function from the auditory nerve to the mesencephalon (Supplementary Fig. S6A) [46]. The amplitude (defined as the difference between the peak and the succeeding trough of wave II) remained unchanged over the course of 6 days (Supplementary Fig. S6B, D). The absolute latency for wave II, which is defined as the time interval between the auditory stimulus and the peak of wave II, became slightly longer in treated animals at 20 mins after the injection (with an average increase of 0.35 ± 0.06 ms, Supplementary Fig. S6C, E), implying slightly decreased auditory nerve activities, which was likely caused by the physical dampening of tympanic membranes (TMs) vibration by the formulation. The absolute latency returned to the average value of untreated animals, i.e., ~ 2.8 ms, after one day post-injection. Overall, the ABR threshold, peak amplitude, and absolute latency of each animal did not exhibit large variations, suggesting that the treatment did not substantially alter the auditory functions of the chinchillas.

Potential tissue toxicity induced by the V_2O_5 NWs treatment was assessed with histological analysis of TMs. Bullae of animals treated with 0.08 mg/mL V_2O_5 NWs and 1 mM Br $^-$ for 7-day were retrieved, the TMs of which were demonstrated to be histologically similar to pristine TMs (Fig. 4D), with the thickness of 25.2 \pm 1.8 mm that is

comparable to healthy TMs ($18.2 \pm 4.5 \,\mathrm{mm}$). No tissue injury, necrosis, or inflammatory cells were identified in the treated groups.

These results demonstrated the excellent biocompatibility of the nanozyme formulation, which, combined with the aforementioned antimicrobial efficacy, hints at a promising treatment for OM that enables on-demand synthesis of therapeutics and targeted eradication of pathogens at the site of infection. That excellent biocompatibility is also consistent with the recent study reporting cytoprotective effect of nanosized V_2O_5 via their glutathione-peroxidase (GPx)-like activities [27].

V₂O₅ NWs/Br- formulation cured OM in vivo in chinchillas

After confirming the in vitro antimicrobial activities and in vivo biocompatibility of the V₂O₅ NWs, a S. pneumoniae-induced chinchilla OM model was used to study the in vivo antimicrobial efficacy of V₂O₅ NWs. Timeline for the procedure used to establish the infection and to collect samples for the in vivo efficacy assessment is shown in Fig. 5 A. In brief, the auditory bullae are dry and sterile under healthy conditions, into which S. pneumoniae was directly inoculated through the dorsal aspect of the bullae on day -3 (where the time of treatment administration was used as day 0). Daily otoscopy was performed to determine the presence of fluid in the auditory bullae and signs of infection, such as bulging TMs and erythema as shown in Fig. 5 B (right). Once abnormality was identified, the MEF of the treated and nontreated animals was collected for serial dilution and culture to quantify the CFU of S. Pneumoniae in the middle ear, for which a value greater than 10⁴ CFU was used as an indication of successful establishment of the infection [26]. That culture of MEF also served as a verification that S. Pneumoniae was the only bacteria identified in the auditory bullae. Identification of other pathogens (e.g., P. aeruginosa) would indicate contamination and thus the animal would be eliminated from the experimental group.

Once infection was established, $200\,\mu\text{L}$ of a formulation containing a PBS-buffered solution of $0.08\,\text{mg/mL}\,V_2O_5$ NWs with $1\,\text{mM}\,Br^-$ or $0.08\,\text{mg/mL}\,V_2O_5$ alone were injected through the auditory bullae, which was considered day 0 of the treatment. V_2O_5 NWs were consistently detected in the MEF over the course of the 7-day

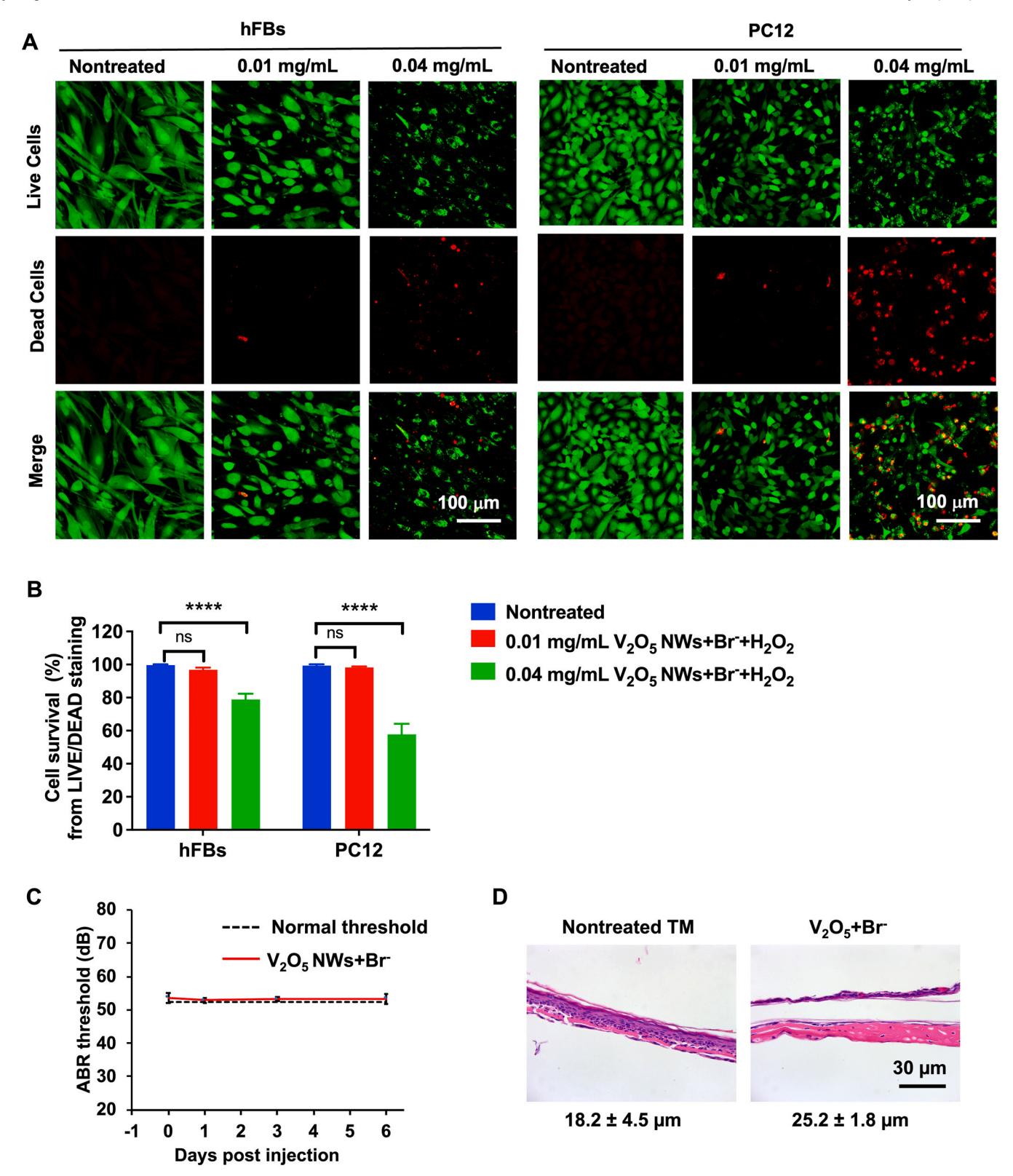


Fig. 4. Biocompatibility assessments in vitro and in vivo. (A) Confocal microscopy images of the LIVE/DEAD staining of hFBs and PC12. Green, live cells; red, dead cells. Cells were incubated with 0.01 mg/mL or 0.04 mg/mL V₂O₅ NWs (as labeled in the figure), 1 mM Br⁻, and 20 μ M H₂O₂ for 24 h. (B) Cell survival rate (%), calculated by counting the live and dead cells in (A). Data are mean \pm SD. n = 4. ns, not statistically significant, **** p < 0.0001. (C) ABR thresholds in response to an acoustic click before and after the treatment with a formulation containing 0.08 mg/mL V₂O₅ NWs and 1 mM Br⁻. The black dashed line indicated the hearing threshold of healthy chinchillas before the treatment. Data are mean \pm SD. (n = 5). (D) The cross-section micrographs of the H&E-stained pristine and treated TMs. The treated TMs were exposed to 0.08 mg/mL V₂O₅ NWs and 1 mM Br⁻ for 7 days⁻

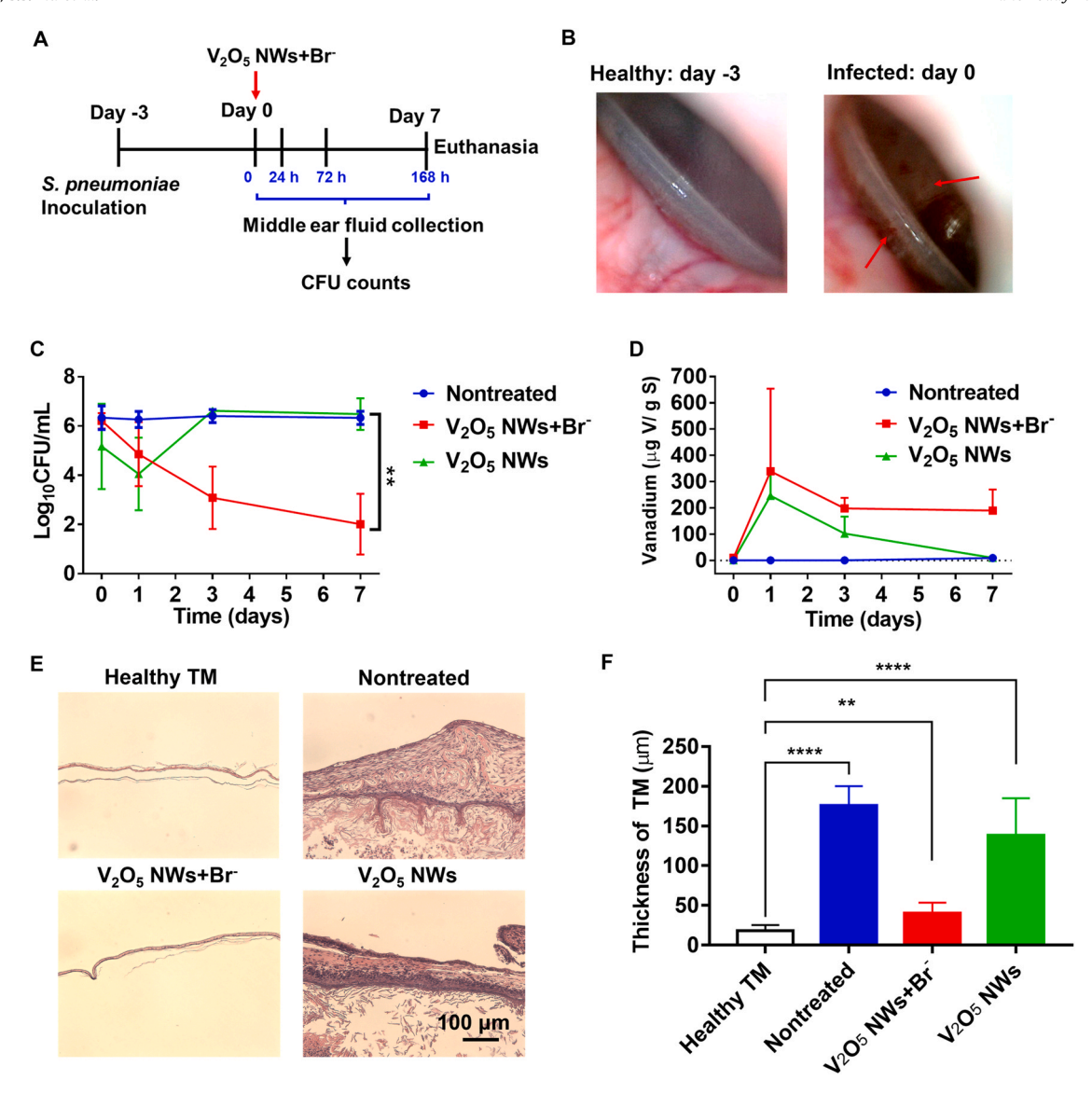


Fig. 5. In vivo therapeutic efficacy of the V_2O_5 NWs in a standard chinchilla OM model. (A) The timeline of the in vivo procedures to induce and treat OM in chinchillas. (B) Otoscope images of the TMs of healthy (left) and infected (right) animals. The red arrows indicated the bulging TM and erythema observed during an OM episode. (C) Time course of the bacterial CFU count in the MEF of animals with OM. The formulations contained 0.08 mg/mL V_2O_5 NWs and/or 1 mM Br $^{\circ}$. Data are mean \pm SD. n = 8 for the nontreated group; n = 5 for the group that received both V_2O_5 NWs and Br $^{\circ}$; n = 4 for the group that only received V_2O_5 NWs. Log₁₀CFU for CFU \sim 0 was set to zero instead of minus infinity for the purpose of illustration. ** p < 0.01. (D) Vanadium content in the MEF of animals with OM, following a single intrabullae injection quantified using ICP-MS (normalized to Sulfur (S), a surrogate for total tissue quantity). Data are mean \pm SD. n = 3-4 for each time point. (E) Representative H&E-stained sections of pristine, infected, and treated TMs. (F) Thicknesses of the TMs, quantified using the H&E-stained sections. Data are mean \pm SD. n = 5. ns, not statistically significant, ** p < 0.01, *** p < 0.0001.

treatment (Fig. 5 D). That successful retention of the V₂O₅ NWs was likely a result of the clogged eustachian tube during (and sometimes following) an active episode of OM, which renders the auditory bulla a closed environment with no liquid drainage [47] (Eustachian tube connects nasopharynx and auditory bulla, which ensures proper liquid drainage and keeps the bulla dry in healthy ears [48].). Furthermore, that liquid environment provided by the MEF is likely needed to sustain the catalytic reactions enabled by the V₂O₅ NWs, as discussed above. MEF was extracted from the dorsal aspect of the auditory bullae at day 1, 3 and 7 to monitor bacteria growth in the middle ear. The number of CFU in the middle ear of the infected animals was reduced by more than 10,000 times in the group that received the V₂O₅ NWs + Br⁻ treatment (Fig. 5 C), which far exceeded the common criteria for complete cure, i.e. 3-log reduction in the middle ear CFU count [25,26]. Despite the in vitro antimicrobial effect of V₂O₅ NWs alone, the formulation only containing 0.08 mg/ mLV₂O₅ NWs did not eradicate S. Pneumoniae OM in vivo.

Substantial presence of V_2O_5 NWs was detected in the middle ear of the treated animals throughout the 7-day treatment via inductively coupled plasma mass spectrometry (ICP-MS) at each time point. As shown in Fig. 5 D, the level of vanadium in the MEF of treated animals was still detectable by day 7 in the group that received the V_2O_5 NWs +Br $^-$ treatment, suggesting that nanowires could be retained in the middle ear for at least 7 days after a single injection.

Histology confirmed the biocompatibility of the treatment in the treated or nontreated infected animals (Fig. 5 E). Thickness of the infected and subsequently treated animals had their TMs return to levels close to the pristine TMs (40.2 \pm 13.2 mm for V_2O_5 NWs + Br'vs 18.2 \pm 7.0 mm for healthy TM) after the 7-day treatment. By comparison, the infected but not treated animals demonstrated TMs with a thickness of 175.7 \pm 24.5 μm , nearly 10 folds that of the pristine TMs (Fig. 5 F).

The 4-log reduction of CFUs in the MEF of infected and treated animals and their post-treatment TMs that appeared similar to the

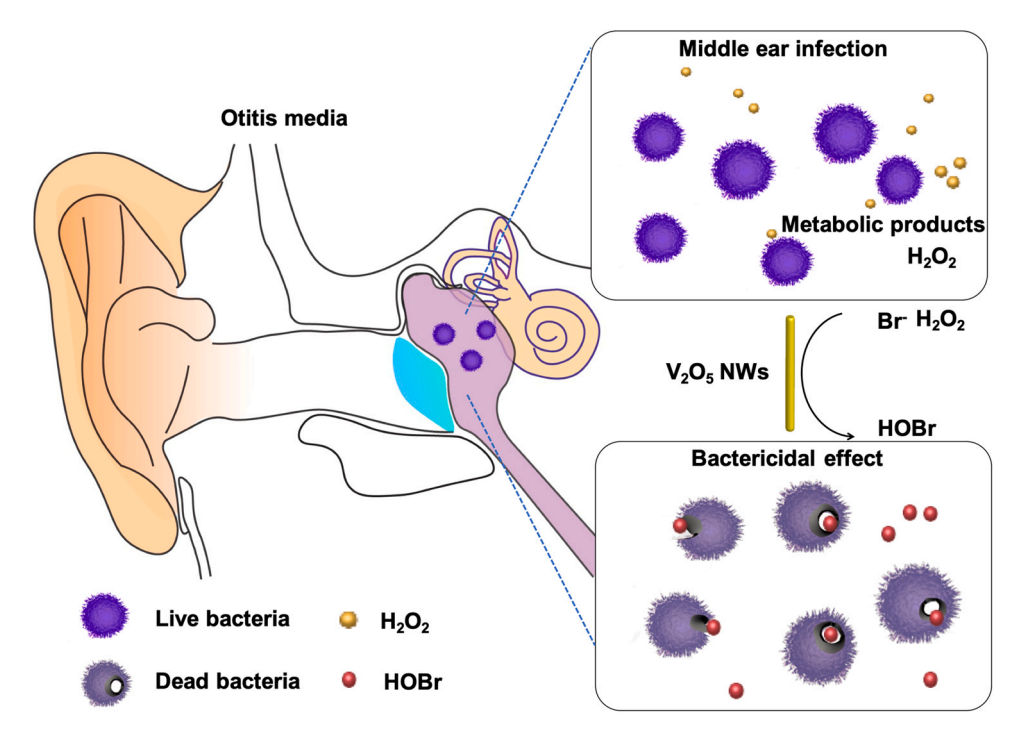


Fig. 6. Schematic diagram of antimicrobial properties of the V_2O_5 NWs for the treatment of otitis media.

pristine ones, demonstrated that the V_2O_5 NWs +Br $^-$ formulation cured S. pneumoniae OM in chinchillas within 7 days without causing severe toxicity. Therefore, the haloperoxidase-mimicking V_2O_5 NWs could replace the conventional antibiotic therapies for OM treatment.

Discussion

We have developed an OM treatment that enabled the synthesis of an antiseptic, HOBr, in a middle ear infected by *S. pneumoniae*, which in turn eradicated the infection. HOBr was generated by oxidizing Br using the $\rm H_2O_2$ produced by the pathogen, catalyzed by $\rm V_2O_5$ NWs (Fig. 6). A single-dose formulation containing $\rm V_2O_5$ NWs and Br effectively cured *S. pneumoniae* OM in an established chinchilla animal model, without causing tissue damages in the ear or impacting on hearing sensitivity. This strategy of converting the metabolic products of pathogens into potent antimicrobials could be applicable to the treatment of other infections caused by *S. pneumoniae*, such as pneumonia and meningitis [28], as well as infections caused by a broad range of $\rm H_2O_2$ -generating pathogens [49], including *Streptococcus pyogenes*, *Streptococcus mutans* and *Streptococcus mitis*.

The antiseptic, HOBr, was chosen based on the broad-spectrum efficacy of hypohalous acids [16] and their long history of application in healthcare and water disinfection without breeding substantial drug resistance [15]. Recently, a selection of antiseptics, including N-chlorotaurine [50], amylmetacresol [51], and thymol [52] has been used to treat topical infections including otitis externa, but few studies have attempted OM treatment with antiseptics due to their short half-life that requires frequent administration to the site of infection, which is challenging to access in the case of OM. That challenge was addressed in this study via the in situ generation of antiseptics.

The central point of this work was the on-demand and self-regulated synthesis of HOBr at the site of infection, enabled by the V_2O_5 NWs, turning the pathogen's own metabolic products against itself. Upon administration of a formulation containing V_2O_5 NWs and Br^- into the middle ear bullae of infected chinchillas. HOBr was

generated continuously while consuming the H_2O_2 produced by *S. pneumoniae*. The HOBr synthesized in situ eradicated the pathogen over the course of 7 days, at which point the production of HOBr ceased automatically, avoiding potential side effects caused by overexposure to the antiseptic.

The treatment design leveraged a key characteristic of S. pneumoniae, i.e., the production of H₂O₂. During the log-phase growth, S. pneumoniae excretes H₂O₂ at a rate up to ~1 mM per hour, enabled by its pyruvate oxidase [19]. Its high tolerance for H_2O_2 thus endows S. pneumoniae with a significant survival advantage over other microbial inhabitants in the middle ear. Converting H₂O₂ to a more potent antiseptic, i.e., HOBr, could thus eradicate S. pneumoniae along with other pathogens. Furthermore, removing the H₂O₂ produced by S. pneumoniae catalytically could have the added benefit of alleviating the suppression of the host immune system. Immune suppression in the middle ear has been reported as a result of the H₂O₂ produced at the mM level, as a result of the inactivation of the inflammasomes in immune cells (e.g., macrophage) caused by H₂O₂ [53]. Although the effect of HOBr on the immunoactivities in the middle ear requires detailed future investigation, the excellent treatment efficacy reported here and the recent discovery of the cytoprotective effect of V₂O₅ nanoparticles [27] hint at potential positive effects on the host immune system.

The in situ conversion of H₂O₂ to HOBr was enabled by the nanozyme, V₂O₅ NWs. Although (per)oxidase-mimicking nanozymes, such as nanosilver, metal oxides, and carbon-based nanostructures have been utilized to replace conventional antibiotics in topical infections [54], most of the (per)oxidase reactions require an acidic environment that are rare in living systems [54]. Unlike the aforementioned nanozymes, the V₂O₅ NWs were chosen in this study based on its analogous catalytic activities as the biological enzyme, V-HPOs, which was identified in seawater (pH 8.3) [30]. Indeed, we demonstrated the high catalytic activities of the V₂O₅ NWs under neutral and alkaline conditions (e.g., the pH of MEF has been reported to be 7.0–8.5 [42]) and excellent antimicrobial efficacy. Despite the reported toxicity of bulk V₂O₅ materials to mammalian cells, biocompatibility has been established in the literature for nanosized particles, such as nanowires, nanospheres, nanoflowers, or

nanosheets including V_2O_5 nanoparticles [27,55]. No inflammation, necrosis, or other tissue damages were identified in our histological analysis on the animals treated with V_2O_5 NWs, in health or disease. The ABR tests further corroborated the biocompatibility of the V_2O_5 NWs, demonstrating nearly identical hearing sensitivity in nontreated and treated animals. Sustained presence of the V_2O_5 NWs throughout the 7-day treatment was demonstrated in animals that received V_2O_5 NWs and Br $^-$, hinting at the potential prophylactic effects of this formulation for recurrent OM. This single-dose treatment has the potential to reduce antibiotic usage and mitigate the development of drug resistance during the treatment of OM.

Potential chronic effects of V₂O₅ NWs and avenues toward bioresorbable analogs remain to be explored in future work. Past reports on inorganic nanowires could provide key inspiration for future designs. For example, silicon nanowires have been shown to be biodegradable and their degradation products, e.g., Si(OH)₄, to be highly biocompatible in cardiac experiments [56]. In one example, the cardiac patch scaffolds containing Si ions were found to stimulate the expression of cardiac-specific genes and the proliferation in primary cardiomyocytes, hinting at enhanced cardiac function upon exposure to silicon nanowires. Moreover, the silicon nanowire fieldeffect transistors are stable in the dry state but can undergo hydrolysis in aqueous solutions [57], which has been leveraged to achieve bioresorbable electronics. As such, one avenue forward to improve bioresorbability of the V₂O₅ NWs could be to leverage the reported biocompatibility of silicon nanowires and coat them with a thin layer of V_2O_5 .

Recent clinical studies that surveyed the etiologic agents in pediatric OM concluded that S. pneumoniae and NTHi are the most prevalent bacterial pathogens [1]. Although this report addressed OM caused by S. pneumoniae, which is considered more challenging to treat due to its high MICs [26], future research should address the treatment of coinfections by S. pneumoniae and NTHi, where HOBr generated by *S. pneumoniae* could be sufficient for the simultaneous eradication of the two pathogens. As HOBr is quite a novel therapeutic when it comes to OM treatment, its potential resistance and resistance development mechanisms are not yet understood, which will undoubtedly become an important focus of our future research. To enable the non-invasive administration of the formulation, the permeation barrier of the TM, which is largely impermeable to all drugs (including small molecules, nanoparticles, and antibodies) [58], needs to be addressed. The previously demonstrated approach of using chemical permeation enhancer (CPEs) to increase the transtympanic drug flux across intact TMs [58,59] or shrinking the size of the V₂O₅ NWs could be effective strategies to enable the noninvasive delivery. Although we did not observe piercing of tissue or cell membranes by the V₂O₅ NWs reported here, biosafety concerns have been raised about carbon nanotubes with similar particle morphologies [60,61]. While not an acute issue in the current study, future research will dissect the individual effect of particle morphology and particle chemistry on their in vivo toxicity. In addition, long-term biocompatibility studies will also be an important focus of future research to unravel the clearance kinetics and mechanisms of V₂O₅ NWs from the middle ear of infected animals and the effect of HOBr on the host immunoactivities.

While the V_2O_5 NWs were designed to treat acute OM caused by *S. pneumoniae*, they could be useful in other OM-related indications. Below we briefly comment on purulent OM and suppurative OM as examples. Purulent OM entails an auditory bulla filled with MEF, which could be due to a bacterial infection or the inflammation reactions that linger after pathogens are eradicated. Based on their efficacy against acute OM, the V_2O_5 NWs could treat purulent OM caused by *S. pneumoniae*. They may have limited effect on non-infectious purulent OM as anti-inflammatory effects of the V_2O_5 NWs have not been studied. Suppurative OM entails TM perforation, which often occurs because of pressure buildup (e.g., from middle

ear fluid) that bursts a tympanic membrane during active or recurring infections. We believe the V_2O_5 NWs could still function well against suppurative OM caused by *S. pneumoniae*. While it is possible that the V_2O_5 NWs could be carried out of the auditory bullae along with the bursting MEF, previous studies have shown that rod-shaped particles have unusually long retention time at the injection site due to their large radius of gyration and thus small diffusivity even under flow of body fluids. It is therefore also possible that the V_2O_5 NWs could remain in the auditory bullae during suppurative OM episodes. If that is the case, the V_2O_5 NWs could be hugely beneficial for the treatment of recurring suppurative OM as they could act as a prophylactic and a treatment measure simultaneously. A detailed investigation into the retention and efficacy of V_2O_5 NWs in other OM types and associated complications will be a central focus of our future work.

In conclusion, we have developed an effective local therapy that enabled on-demand synthesis of therapeutics that cured *S. pneumoniae*-induced OM in the standard chinchilla model. It was formulated for a convenient and single-dose local injection, which generates the antiseptic, HOBr, autonomously upon emergence of the pathogen *S. pneumoniae* and ceases that synthesis upon pathogen eradication, yielding excellent biocompatibility in the ear. This stand-alone nanomedicine was designed to replace conventional antibiotics in the treatment of OM, an extremely common pediatric condition, thereby reducing the exposure to antibiotics and associated side effects and curbing the development of drug resistance. The strategy of using nanozymes for the in situ and ondemand synthesis of antiseptics provides a new paradigm for the treatment of local infectious diseases.

Methods

Preparation of V₂O₅ NWs

V₂O₅ NWs were synthesized through a hydrothermal method as previously described [30,32]. VOSO₄.nH₂O (purity > 99.9 %), KBrO₃ (purity > 98 %), and nitric acid (purity ≥65 %) were used as received from Alfa Aesar, Sigma Aldrich, and Trace SELECT* Ultra respectively. In short, VOSO₄.nH₂O (8 mmol) and KBrO₃ (5 mmol) were dissolved and stirred continuously in distilled water (30 mL) at room temperature for 30 min. Nitric acid was added to the stirring solution dropwise until a pH of 1–2 was reached. Then the solution was transferred to a Teflon-lined stainless-steel autoclave for a reaction period of 24 h at 180 °C. After the autoclave was cooled down to room temperature naturally, the solution was filtered and washed with distilled water followed by ethanol for several times. The resulting dark-yellow nanomaterial was dried at 80 °C overnight under vacuum and then evaluated by the following characterization technique, as described in Supplementary Materials and Methods.

Bromination activity

The bromination activity was measured for 10 min at 37 °C in PBS buffer or Milli-Q water by varying the concentration of the V_2O_5 NWs (0–0.08 mg/mL) and with constant concentration of PR (25 μ M), Br⁻ (1 mM) and H₂O₂ (10 μ M). Potassium bromide (KBr) was used to provide Br⁻. V_2O_5 NWs were added to the mixture immediately prior to the measurements to trigger the reaction. The concentration of Br₄PR was calculated using the Lambert-Beer Law with an extinction coefficient (590 nm) of $\varepsilon_{\rm Br4PR}$ to be 72,200 M⁻¹CM⁻¹. In order to measure the Michaelis-Menten kinetics, two independent set of experiments were performed: 1) Br⁻ concentration was varied (0–20 mM) while keeping concentrations of V_2O_5 NWs (0.04 mg/mL), H₂O₂ (10 μ M) and PR (25 μ M) constant. 2) H₂O₂ concentration was varied (0–600 μ M) while keeping the concentration of V_2O_5 NWs (0.04 mg/mL), Br⁻ (1 mM) and PR (25 μ M)

constant. For each measurement, blank tests and controls were performed, each measurement was carried out 3 times. The values were fitted to the Michaelis–Menten model and kinetic parameters were determined by Lineweaver–Burk linearization.

Turnover frequency (TOF)

The turnover frequency (TOF = k_{cat}) was calculated as the maximum formation rate per minute (v_{max}) of PR for molar concentrations of the catalyst and a concentration of 219.9 μ M V_2O_5 NWs (0.04 mg·mL⁻¹/181.88 g·mol⁻¹) and yield to 4.2 × 10⁻⁴ min⁻¹. As the oxidative bromination of PR requires the oxidation of four Br⁻, the TOF with respect to the HOBr concentration is 1.7 × 10⁻³ min⁻¹.

Stability assay

The stability assay was carried out by incubating 0.04 mg/mL V_2O_5 NWs with 1 mM Br $^{-}$, $10\,\mu\text{M}\,H_2O_2$ in Milli-Q water at 37 °C. After each reaction time (1, 2, 3, 4, 6, 8 and 12 h), The reaction was terminated by centrifuging the suspension for 5 min at 10 000 g, then the V_2O_5 NWs were collected, washed with Milli-Q-water and treated again with 1 mM Br $^{-}$, $10\,\mu\text{M}\,H_2O_2$ in Milli-Q water under identical experimental conditions. 10 mins after each time point, $10\,\mu\text{L}$ of aliquots were taken to calculated ν_0 .

Antibacterial test

S. pneumoniae was incubated in brain heart infusion (BHI) broth (BD biosciences) at 37 °C with 5 % CO₂ until the mid-log phase. Then the bacteria were treated with five different formulations for 15 h: nontreated, Br $^-$ +H₂O₂, V₂O₅ NWs, V₂O₅ NWs+Br $^-$ and V₂O₅ NWs+Br $^-$ +H₂O₂. The concentrations of various species in the formulations were V₂O₅ NWs (0.04 mg/mL), Br $^-$ (1 mM) and H₂O₂ (20 μ M). The optical density at 600 nm was measured as a function of time. Subsequently, S. pneumoniae was plated on blood agar (TSA with Sheep Blood, Thermo ScientificTM RemelTM) plates, and left to grow for 15 h at 37 °C with 5 % CO₂.

Cytotoxicity analysis

Human primary dermal fibroblasts (hFBs, ATCC PCS-201-012) were maintained in Fibroblast Basal Medium (FBM, ATCC PCS-201-020) with Fibroblast Growth Kit - Low Serum (ATCC, PCS-201-041) and 1 % penicillin/streptomycin (Gibco) at 37 °C with 5 % CO₂. The pheochromocytoma cell line (PC-12) was maintained in ATCC-formulated F-12 K medium with 2.5 % fetal bovine serum (Gibco), 15 % horse serum (Gibco) and 1 % penicillin/streptomycin (Gibco) at 37 °C with 5 % CO₂. Once seeded hFBs and PC12 were seed in 96 well plates (Corning Costar) at a density of 5000 cells/well, the V₂O₅ NWs (with 1 mM Br and 20 μ M H₂O₂) were introduced into the cells above and then incubated for 24h. Cell survival rate was tested using a LIVE/DEAD Viability/Cytotoxicity Kit (Molecular Probes, Invitrogen). Cells were incubated with calcein-AM (acetoxymethyl) (1 mM) and ethidium homodimer-1 (2 mM) for 30 min at 37 °C to label live and dead cells, respectively. Cell survival rate (%) was calculated as live cells/(live cells + dead cells) \times 100.

Animal maintenance

Healthy adult male chinchillas from Mutation Chinchilla Breeder Association (NY) were used with weights between 500 and 650 g. The animals were kept in cages in a group of two with free access to water and food and cared according to the protocols approved institutionally and nationally. Experiments were conducted and approved by the Institutional Animal Care and Use Committee (IACUC)

in conjunction with the Cornell University Center of Animal Resources and Education (CARE) Animal Use Guidelines.

ABR measurements

A custom program written in LabView (Laboratory Virtual Instrument Engineering Workbench, National Instruments, Austin, Texas, USA) was used to control the auditory stimulus, and to acquire, filter, and store the ABR data. ABR response was collected via subdermally-placed platinum-iridium needle electrodes (Astro-Med Grass Instruments, West Warwick, Rhode Island, USA). The active electrode was placed at the cranial vertex, the reference electrode at the ventrolateral side of each ear, and the ground electrode at the dorsum of the animal. The auditory stimulus was delivered through a sealed headphone which was placed inside the external ear canal of the tested ear. A balanced click was delivered every second, with a duration of 0.2 ms. Stimulus started at 0.1 mV and incremented at step size of 0.1 mV or more. ABR signals were passed to an amplifier (AC amplifer model CP511, Astro-Med Grass Instruments). The signals were amplified with a gain of 200,000 and filtered with lowand high-pass filters of 3000 Hz and 300- Hz, respectively. Measurements were taken at a stimulus frequency of 21 Hz and 1000 acquisitions cycles were averaged. Animals were anesthetized with vaporized isoflurane in oxygen for the duration of the ABR testing and monitored until recovery from anesthesia. Baseline measurements were obtained for each ear prior to the trans-bullar injection of 0.08 mg/mL V₂O₅ NWs and 1 mM Br⁻ in PBS buffer (200 µL). Subsequent ABR measurements were taken at the following timepoints: 20 min, 1 day, 3 days, and 6 days after formulation injection. Animals were euthanized on day 6 after the ABR test and the bullae were retrieved for histological analysis. ABR threshold was analyzed post-measurement and compared to the baseline measurement of each ear.

S. pneumoniae OM chinchilla model

All procedures were conducted in accordance with the Cornell University CARE and approved by the IACUC. Once grown to the midlog phase, isolates of S. pneumoniae were diluted in Hanks' balanced salt solution (HBSS), and then the mixed solution (100 mL, 25–75 CFU) was inoculated directly into each middle ear through the bullae under aseptic conditions. The number of inoculated ears per chinchilla was based on experimental needs. Once pathogens were introduced, assessments of each middle ear were performed by using otoscopy daily, and body weights were recorded as well. Once the middle ear infection was established (usually after 4 days of inoculation), the drug containing nanowires (a PBS-buffered solution of 0.08 mg/mL V_2O_5 NWs and 1 mM Br⁻) were given through ear bullae under aseptic conditions. Direct samples of middle ear culture were collected with calcium alginate swabs and subsequently streaked onto blood agar plates. MEF samples for bacteria culture were collected with a 22-gauge angiocatheter connected to a tuberculin syringe during aseptically surgical procedures with painkillers (nalbuphine) at different time points (day 0, day1, day3, day 7). The MEF (10 mL) of each ear was diluted 1:10 in HBSS, and 3-4 serial 10-fold dilutions were prepared as well. 10 mL of each dilution was pipetted onto the blood agar plates and the number of colonies was counted later to calculate CFU. The lower limit for detecting organisms by using this dilution method in the MEF was 100 CFU/mL.

Histopathology

7 days after formulations were administrated through the bullae, animals were euthanized. Following the sacrifice, TMs were excised and immediately fixed in 10 % neutral buffered formalin overnight,

then decalcified, embedded in paraffin, sectioned (5-µm thick), and stained with H&E by the Section Anatomic Pathology Histology Laboratory at Cornell University (Ithaca, New York, USA; fee for service), using standard techniques. All stained specimens were evaluated under light microscopy. The thickness of TMs was measured by Image I software.

MEF collection for ICP-MS

Chinchilla's MEF was extracted at 1 day, 3 days and 7 days after giving treatment, and all samples were stored at -80 °C until analysis. The ICP-MS analysis was performed by Trace Element Research Group at UW-Madison & Wisconsin State Laboratory of Hygiene. Samples for analysis by a magnetic sector inductively coupled plasma mass spectrometry (Thermo-Finnigan Element XR) were labeled only by a unique identifying number, so the investigators performing the analyses were blinded to the treatment group. Vanadium measurements were performed using an ICP-MS. For sample preparation, 20 or 40 µL of samples were digested by 100 µL Tetramethylammonium hydroxide (TMAH) at 85 °C for 18 h. Digested samples were then diluted with 10 % nitric acid to a final volume of 1.2 mL for ICP-MS analysis prior to running. A quantitative analysis method in standard mode measuring the vanadium 51 isotope was used to determine vanadium concentrations in MEF. Gallium 70 isotope was used as the internal standard. Each sample was run in triplicate and vanadium concentrations were normalized to major elements in the MEF (Na, Ca, Mg, P). Mean batch-specific analytical blank (with outlier detection) applied to all sample data. Propagated uncertainty estimates for each sample/element include: (a) ICP-MS analysis (standard deviation of triplicate analyses on each sample) and (b) blank subtraction (standard deviation of 4 method blanks from each batch). The comprehensive QA/QC ensures that robust data were produced, and all internal and external QA/QC was acceptable.

Detection of H₂O₂ production

After culturing S. pneumoniae for about 15 h, the suspension was collected and tested using a H₂O₂ fluorometric assay kit named Hydrogen Peroxide Assay Kit from Cayman Chemical. Briefly, H₂O₂ was detected using 10-acetyl-3,7-dihydroxyphenoxazine (ADHP), a highly sensitive and stable probe for H₂O₂. In a horseradish peroxidase catalyzed reaction, ADHP reacts with H₂O₂ with a 1:1 stoichiometry to produce highly fluorescent resorufin. The resorufin fluorescence can be detected using an excitation wavelength of 530 nm and an emission wavelength of 590 nm. The detected fluorescence was then compared with standard curve of H₂O₂ to get exact amount of H₂O₂ production.

Statistical analysis

Data were analyzed using Graphpad Prism software (version 7.0) and presented as the mean ± SD. One-way ANOVA followed by Tukey's HSD test was applied for comparison between two groups or among multiple groups; ns, not statistically significant, **p < 0.01, **** p < 0.0001.

Funding

This work was supported by the Department of Defense, Office of Naval Research (ONR award N00014- 20-1-2418); National Institutes of Health, National Institute on Deafness and Other Communication Disorders (NIHDC016644).

CRediT authorship contribution statement

I.L. and **R.Y.** conceived the idea and designed the experiments. J.L., M.S. and T.F. synthesized the nanoparticles. J.L. and X.M. conducted the nanoparticles characterization (XPS, TEM, XRD) and the in vitro experiments. J.L., X.M., S.L. and D.S. performed the in vivo experiments. E.L., I.L., S.L., and X.M. performed the ABR test. R.Y. supervised the study. The manuscript was prepared by **I.L. X.M.** and **R.Y. J.L.** and **X.M.** contributed equally to this work.

Data availability

The authors declare that the main data supporting the findings of this study are available within the article and its Supplementary Materials files. Extra data about this study are available from the corresponding author upon request.

Declaration of Competing Interest

The authors declare that they have no known competing financial interests or personal relationships that could have appeared to influence the work reported in this paper.

Acknowledgements

This work made use of the Cornell Center for Materials Research (CCMR) Shared Facilities which are supported through the NSF MRSEC program (DMR-1719875). We thank CCMR staff members J. Grazul for his assistance with acquiring TEM and HRTEM images and performing STEM-EDX measurements, and D. Johnson-McDaniel for her assistance during XPS data collection. We thank the Trace Element Research Group at University of Wisconsin-Madison for providing access to ICP-MS measurements. We thank S. Pelton at Boston University School of Medicine and Publica Health and Boston Medical Center for gifting us the clinical isolate of *S. pneumoniae*.

Appendix A. Supporting information

Supplementary data associated with this article can be found in the online version at doi:10.1016/j.nantod.2022.101672.

References

- [1] N. Shirai, D. Preciado, Curr. Opin. Otolaryngol. Head Neck Surg. 27 (2019)
- [2] R. Mittal, J.M. Parrish, M. Soni, J. Mittal, K. Mathee, J. Med. Microbiol 67 (2018) 1417-1425.
- [3] S. Hullegie, R.P. Venekamp, T.M.A. van Dongen, A.D. Hay, M.V. Moore, P. Little, A.G.M. Schilder, R. Damoiseaux, Pediatr. Infect. Dis. J. 40 (2021) 756-762.
- [4] A. Hoberman, J.L. Paradise, H.E. Rockette, D.H. Kearney, S. Bhatnagar, T.R. Shope, J.M. Martin, M. Kurs-Lasky, S.J. Copelli, D.K. Colborn, S.L. Block, J.J. Labella, T.G. Lynch, N.L. Cohen, M. Haralam, M.A. Pope, J.P. Nagg, M.D. Green, N. Shaikh, N. Engl. J. Med. 375 (2016) 2446-2456.
- [5] J.A. Ayukekbong, M. Ntemgwa, A.N. Atabe, Antimicrob. Resist Infect. Control 6 (2017) 47-47.
- J. Davies, G.B. Spiegelman, G. Yim, Curr. Opin. Microbiol. 9 (2006) 445-453.
- C. Bergenfelz, A.P. Hakansson, Curr. Otorhinolaryngol. Rep. 5 (2017) 115-124.
- [8] M.K. Van Dyke, J.-Y. Pirçon, R. Cohen, S.A. Madhi, A. Rosenblüt, M. Macias Parra, K. Al-Mazrou, G. Grevers, P. Lopez, L. Naranjo, F. Pumarola, N. Sonsuwan, W.P. Hausdorff, Pediatr. Infect. Dis. J. 36 (2017) 274–281.
- Y. Hirakata, K. Ohmori, M. Mikuriya, T. Saika, K. Matsuzaki, M. Hasegawa, M. Hatta, N. Yamamoto, H. Kunishima, H. Yano, M. Kitagawa, K. Arai, K. Kawakami, I. Kobayashi, R.N. Jones, S. Kohno, K. Yamaguchi, M. Kaku, Antimicrob. Agents Chemother. 53 (2009) 4225–4230.
- [10] N. Littorin, J. Ahl, F. Udden, F. Resman, K. Riesbeck, BMC Infect. Dis. 16 (2016) 407.
- S.N. Patel, A. McGeer, R. Melano, G.J. Tyrrell, K. Green, D.R. Pillai, D.E. Low, Antimicrob. Agents Chemother. 55 (2011) 3703-3708.
- [12] Centers for Disease Control and Prevention, (2013) 1-114.
- N.B. Halasa, M.R. Griffin, Y.W. Zhu, K.M. Edwards, J. Pediatr. 144 (2004) 200–205. H.M. Massa, A.W. Cripps, D. Lehmann, Med. J. Aust. 191 (2009) S44-S49.
- W.A. Rutala, D.J. Weber, Clin. Microbiol. Rev. 10 (1997) 597-610.
- [16] P. Magee, Side Eff. Drugs Annu. 33 (2011) 479-490.

- [17] R. Wever, M.G.M. Tromp, B.E. Krenn, A. Marjani, M. Van Tol, Environ. Sci. Technol. 25 (1991) 446–449.
- [18] B. Halliwell, M.V. Clement, L.H. Long, FEBS Lett. 486 (2000) 10-13.
- [19] J.P. Lisher, H.-C.T. Tsui, S. Ramos-Montañez, K.L. Hentchel, J.E. Martin, J.C. Trinidad, M.E. Winkler, D.P. Giedroc, mSphere 2 (2017) e00291–00216.
- [20] M. Giorgio, M. Trinei, E. Migliaccio, P.G. Pelicci, Nat. Rev. Mol. Cell Biol. 8 (2007) 722–728.
- [21] P. Niethammer, C. Grabher, A.T. Look, T.J. Mitchison, Nature 459 (2009) 996–999.
- [22] M. Yazdanbakhsh, C.M. Eckmann, D. Roos, J. Immunol. 135 (1985) 1378–1384.
- [23] Clare L. Hawkins, Essays Biochem. 64 (2019) 75–86.
- [24] L.O. Bakaletz, Expert Rev. Vaccin. 8 (2009) 1063-1082.
- [25] V. Sabharwal, M. Figueira, S.I. Pelton, M.M. Pettigrew, Microbes Infect. 14 (2012) 712–718.
- [26] R. Yang, V. Sabharwal, N. Shlykova, O.S. Okonkwo, S.I. Pelton, D.S. Kohane, JCI Insight 3 (2018).
- [27] A.A. Vernekar, D. Sinha, S. Srivastava, P.U. Paramasivam, P. D'Silva, G. Mugesh, Nat. Commun. 5 (2014) 5301.
- [28] Centers for Disease Control and Prevention, (2019).
- A. Cassini, L.D. Högberg, D. Plachouras, A. Quattrocchi, A. Hoxha, G.S. Simonsen, M. Colomb-Cotinat, M.E. Kretzschmar, B. Devleesschauwer, M. Cecchini, D.A. Ouakrim, T.C. Oliveira, M.J. Struelens, C. Suetens, D.L. Monnet, R. Strauss, K. Mertens, T. Struyf, B. Catry, K. Latour, I.N. Ivanov, E.G. Dobreva, A. Tambic Andraševic, S. Soprek, A. Budimir, N. Paphitou, H. Žemlicková, S. Schytte Olsen, U. Wolff Sönksen, P. Märtin, M. Ivanova, O. Lyytikäinen, J. Jalava, B. Coignard, T. Eckmanns, M. Abu Sin, S. Haller, G.L. Daikos, A. Gikas, S. Tsiodras, F. Kontopidou, Á. Tóth, Á. Hajdu, Ó. Guólaugsson, K.G. Kristinsson, S. Murchan, K. Burns, P. Pezzotti, C. Gagliotti, U. Dumpis, A. Liuimiene, M. Perrin, M.A. Borg, S.C. de Greeff, J.C.M. Monen, M.B.G. Koek, P. Elstrøm, D. Zabicka, A. Deptula, W. Hryniewicz, M. Caniça, P.J. Nogueira, P.A. Fernandes, V. Manageiro, G.A. Popescu, R.I. Serban, E. Schréterová, S. Litvová, M. Štefkovicová, J. Kolman, I. Klavs, A. Korošec, B. Aracil, A. Asensio, M. Pérez-Vázquez, H. Billström, S. Larsson, J.S. Reilly, A. Johnson, S. Hopkins, Lancet Infect. Dis. 19 (2019) 56–66.
- [30] F. Natalio, R. Andre, A.F. Hartog, B. Stoll, K.P. Jochum, R. Wever, W. Tremel, Nat. Nanotechnol. 7 (2012) 530–535.
- [31] R. André, F. Natálio, M. Humanes, J. Leppin, K. Heinze, R. Wever, H.C. Schröder, W.E.G. Müller, W. Tremel, Adv. Funct. Mater. 21 (2011) 501–509.
- [32] F. Zhou, X. Zhao, C. Yuan, L. Li, Cryst. Growth Des. 8 (2008) 723–727.
- [33] A.A. Akande, A.G.J. Machatine, B. Masina, G. Chimowa, B. Matsoso, K. Roro, M.M. Duvenhage, H. Swart, J. Bandyopadhyay, S.S. Ray, B.W. Mwakikunga, J. Phys. D Appl. Phys. 51 (2018).
- [34] D. Goodacre, M. Blum, C. Buechner, H. Hoek, S.M. Gericke, V. Jovic, J.B. Franklin, S. Kittiwatanakul, T. Söhnel, H. Bluhm, K.E. Smith, J. Chem. Phys. 152 (2020) 044715.
- [35] K. Herget, P. Hubach, S. Pusch, P. Deglmann, H. Götz, T.E. Gorelik, I.Y.A. Gural'skiy, F. Pfitzner, T. Link, S. Schenk, M. Panthöfer, V. Ksenofontov, U. Kolb, T. Opatz, R. André, W. Tremel, Adv. Mater. 29 (2017) 1603823.

- [36] H. Gallard, F. Pellizzari, J.P. Croue, B. Legube, Water Res. 37 (2003) 2883–2892.
- [37] C.D. Pericone, S. Park, J.A. Imlay, J.N. Weiser, J. Bacteriol., 185 (2003) 6815–6825.
- [38] Z. Hasan, R. Renirie, R. Kerkman, H.J. Ruijssenaars, A.F. Hartog, R. Wever, J. Biol. Chem. 281 (2006) 9738–9744.
- [39] E. de Boer, R. Wever, J. Biol. Chem. 263 (1988) 12326-12332.
- [40] A. Frank, C.J. Seel, M. Groll, T. Gulder, ChemBioChem 17 (2016) 2028–2032.
- [41] A.V. Restrepo, B.E. Salazar, M. Agudelo, C.A. Rodriguez, A.F. Zuluaga, O. Vesga, BMC Microbiol. 5 (2005) 34-34.
- [42] R. Osgood, F. Salamone, A. Diaz, J.R. Casey, P. Bajorski, M.E. Pichichero, Laryngoscope 125 (2015) 2204–2208.
- [43] M. Trevino, E. Lobarinas, A.C. Maulden, M.G. Heinz, J. Acoust. Soc. Am. 146 (2019) 3710-3710.
- [44] B.M. Peters, M.A. Jabra-Rizk, G.A. O'May, J.W. Costerton, M.E. Shirtliff, Clin. Microbiol. Rev. 25 (2012) 193–213.
- [45] C. Brown, Lab. Anim. 36 (2007) 22-23.
- [46] G.A. Bargen, Am. J. Audiol. 24 (2015) 573-583.
- [47] R.H. Margolis, P.L. Schachem, L.L. Hunter, C. Sutherland, Audiology 34 (1995) 232–247.
- [48] P. Fireman, J. Allergy Clin. Immunol. 99 (1997) S787–S797.
 - [49] S. Redanz, X.Q. Cheng, R.A. Giacaman, C.S. Pfeifer, J. Merritt, J. Kreth, Mol. Oral Microbiol. 33 (2018) 337–352.
 - [50] A. Neher, M. Nagi, E. Appenroth, M. Gstottner, M. Wischatta, F. Reisigl, M. Schindler, H. Ulmer, K. Stephan, Laryngoscope 114 (2004) 850–854.
- [51] J.S. Oxford, R. Lambkin, I. Gibb, S. Balasingam, C. Chan, A. Catchpole, Antivir. Chem. Chemother. 16 (2005) 129–134.
- [52] A. Sivropoulou, E. Papanikolaou, C. Nikolaou, S. Kokkini, T. Lanaras, M. Arsenakis, J. Agric. Food Chem. 44 (1996) 1202–1205.
- [53] S.F. Erttmann, N.O. Gekara, Nat. Commun. 10 (2019) 3493.
- [54] Z.W. Chen, Z.Z. Wang, J.S. Ren, X.G. Qu, Acc. Chem. Res. 51 (2018) 789-799.
- [55] S. Ghosh, P. Roy, N. Karmodak, E.D. Jemmis, G. Mugesh, Angew. Chem. Int. Ed. 57 (2018) 4510–4515.
- [56] O.A. Bolonduro, B.M. Duffy, A.A. Rao, L.D. Black, B.P. Timko, Nano Res. 13 (2020) 1253–1267
- [57] H. Liu, B. Haider, H.R. Fried, J. Ju, O. Bolonduro, V. Raghuram, B.P. Timko, Nano Res. 11 (2018) 5372–5399.
- [58] R. Yang, V. Sabharwal, O.S. Okonkwo, N. Shlykova, R. Tong, L.Y. Lin, W. Wang, S. Guo, J.J. Rosowski, S.I. Pelton, D.S. Kohane, Sci. Transl. Med. 8 (2016).
- [59] X.J. Khoo, E.J. Simons, H.H. Chiang, J.M. Hickey, V. Sabharwal, S.I. Pelton, J.J. Rosowski, R. Langer, D.S. Kohane, Biomaterials 34 (2013) 1281–1288.
- [60] X. Liu, R.H. Hurt, A.B. Kane, Carbon 48 (2010) 1961–1969.
- [61] T. Thurnherr, C. Brandenberger, K. Fischer, L. Diener, P. Manser, X. Maeder-Althaus, J.-P. Kaiser, H.F. Krug, B. Rothen-Rutishauser, P. Wick, Toxicol. Lett. 200 (2011) 176–186.